The Flow Hydrodynamics Around Tandem Cylinders

Ainal Hoque Gazi and Mohammad Saud Afzal

1 Introduction

From life science to engineering applications, turbulent flows are found everywhere in daily life. The practical application of flow past a bluff body in the domain of thermal and structure system is huge, some of the related such applications can be observed in [1–4]. A flow field is considered either laminar or turbulent based on Reynolds number, which is the ratio of the inertia force to the viscous force. With the change of Reynolds number, the random motion of fluid develops a variation in velocity and pressure [5]. Consequently, the momentum, the mass, and the energy of the flowing fluids are exchanged. The largest turbulent eddies interact with the mean flow and extract energy from it through a process known as vortex stretching. The angular momentum of the larger eddies is conserved during the process of vortex stretching, which maintains turbulence in the flow. Over time these large eddies become unstable and break into further smaller eddies. In this process, there is a cascading of energy from small to the smallest eddies. The energy cascading stops when the Reynolds number of the smallest eddies becomes unity. At this point, the viscosity dominates, and the energy dissipation occurs [6] and the intensity of the turbulence becomes more acute.

The turbulence created around the bridge pier loosens the sediment particles around the pier and the sediments are carried away from the vicinity of the pier, resulting in scour formation. The scour is considered as one of the major reasons behind the failure of bridges. The recent studies dealing with the scour are but not limited to [7–9]. To analysis this, fluid engineers require a potent tool for simulating the turbulence around the pier. Generally, Reynolds Averaged Navier Stokes (RANS), Large Eddy Simulation (LES), Direct Numerical Simulation (DNS) are used to model the turbulence phenomenon. In RANS model, the mean flow and the

A. H. Gazi (✉) · M. S. Afzal
Department of Civil Engineering, Indian Institute of Technology Kharagpur, Kharagpur, India

D. K. Maiti et al. (eds.), *Recent Advances in Computational and Experimental Mechanics, Vol II*, Lecture Notes in Mechanical Engineering,
https://doi.org/10.1007/978-981-16-6490-8_20

impact of the turbulence on the mean flow are the main features, which need a closure rule. The Boussinesq hypothesis are the classical closure method, which were formulated in 1872. Also in the RANS model, no care is taken when smoothing out the model equation, meaning the whole spectrum of the fluctuations are averaged out, and no special preference is given to any mode or scale. A different procedure for modeling more strong eddies is the LES. In LES, a filter is added to the vector fields which remove the specific fluctuating modes. Thus LES captures larger eddies by considering space filtering of the Navier Stokes equations in spite of time averaging.

In this paper, a comparative study of the flow hydrodynamics around tandem cylinders have been carried out using OpenFOAM toolbox for circular cylinders. The RANS and LES models are applied to observe flow hydrodynamics around tandem cylinders. The authors found that the study of flow around the tandem cylinder for both RANS and LES in the same study in an open channel flow is limited. Here, the authors have presented a detailed study of the flow physics around two tandem cylinder mainly highlighting the behavior of force coefficients and the vorticity with the variation of Reynolds number and gap ratios. This study can be further enhanced by performing laboratory experiment for further confirmation.

2 Numerical Model

The simulations presented in this paper are carried out in OpenFOAM5.0, which is a freely available source of C++ codes [10]. PisoFoam, an editable solver in OpenFOAM, was chosen for the purpose of simulation, which solves three-dimensional Navier–Stokes equations (NSE) for a transient, incompressible and turbulent flow. The solver is based on a finite-volume method and PISO (pressure-implicit with the splitting of operators) algorithm for pressure–velocity coupling. For the convective terms in the Navier Stokes equation, the central difference scheme is used; for pressure gradient and inviscid conditions, fourth-order accuracy is applied; for time integration, second-order implicit Euler method is applied. The volume of fluid (VOF) is used to capture the air–water interface. Further, a fraction function, α, is defined as the volume fraction of water in each cell. α is 0 means the cell is filled with air, and α is 1 means the cell is occupied by water; otherwise, $0 < \alpha < 1$ means cells are bisected by the free water surface.

The continuity and the Navier Stokes equation, in their simplified form, adopted in OpenFOAM are given by Eqs. (1) and (2).

$$\frac{\partial u_i}{\partial x_i} = 0 \tag{1}$$

$$\frac{\partial u_i}{\partial t} + u_j \frac{\partial u_i}{\partial x_j} = -\frac{1}{\rho}\frac{\partial p}{\partial x_i} + \frac{\partial}{\partial x_j}\left[(\nu + \nu_t)\left(\frac{\partial u_i}{\partial x_j} + \frac{\partial u_j}{\partial x_i}\right)\right] + g_i \tag{2}$$

where u is time-averaged velocity, p is pressure component, v is eddy viscosity, v_t is kinematic eddy viscosity and g_i is the body force.

2.1 Rans

RANS reduces the computational cost by averaging the flow quantity. In RANS equations the main focus is given to model the Reynolds stress $-\rho u_i u_j$. The turbulence closure is provided by k–ε [11] model as given by Eqs. (3) and (4).

$$\frac{\partial k}{\partial t} + u\frac{\partial k}{\partial x} + v\frac{\partial k}{\partial y} + w\frac{\partial k}{\partial z} = \frac{\partial}{\partial z}\left(\frac{v_t}{\sigma_k}\frac{\partial k}{\partial z}\right) + v_t\left(\left(\frac{\partial u}{\partial z}\right)^2 + \left(\frac{\partial v}{\partial z}\right)^2\right) - \varepsilon \quad (3)$$

$$\frac{\partial \varepsilon}{\partial t} + u\frac{\partial \varepsilon}{\partial x} + v\frac{\partial \varepsilon}{\partial y} + w\frac{\partial \varepsilon}{\partial z} = \frac{\partial}{\partial z}\left(\frac{v_t}{\sigma_\varepsilon}\frac{\partial \varepsilon}{\partial z}\right) + C_{\varepsilon 1}\frac{\varepsilon}{k}v_t\left(\left(\frac{\partial u}{\partial z}\right)^2 + \left(\frac{\partial v}{\partial z}\right)^2\right) - C_{\varepsilon 2}\frac{\varepsilon^2}{k} \quad (4)$$

where k is the turbulent kinetic energy and ε is the turbulent dissipation rate. The eddy viscosity is expressed by Eq. (5).

$$v_t = C_1\frac{k^2}{\varepsilon} \quad (5)$$

For the non-linear k-ε model, the following Boussinesq hypothesis is assumed to model the Reynolds stress ($\tau_{i,j}$)

$$\tau_{i,j} = 2v_t S_{i,j} - \frac{2}{3}k\partial_{i,j} \quad (6)$$

where $S_{i,j}$ is the average strain rate tensor. Constants for Eqs. (3), (4) and (5) have been used from [12], i.e., C_1,$C_{\varepsilon 1}$, $C_{\varepsilon 2}$, σ_k, $\sigma_\varepsilon = 0.09$, 1.44, 1.92, 1.0 and 1.3, respectively. First, the model geometry is defined, and meshes are constructed in blockMesh, with all the necessary boundary conditions in the respective directions. After setting all other parameters, simulation is started by the command PisoFOAM (the name of the solver in openFOAM is treated as a simulating command). The final results are viewed in third-party software paraview. The density of water is taken as 1000 kg/m^3 and the dynamic viscosity of the water is considered as 1.002×10^{-3} kg m^{-1} s^{-1} and kept constant for all of the cases.

2.2 Les

The LES has the capability to solve the 3D turbulence flow condition. The small eddies created in the flow field are modelled by sub-grid scale model, whereas the large scale eddies are calculated directly in the LES. To make this demarcation between small scale and large scale eddies, a filter function is used in NSE. The main equations in LES are obtained by filtering the NSE, as given below-

$$\frac{\partial \overline{u_i}}{\partial x_i} = 0 \tag{7}$$

$$\frac{\partial \overline{u_i}}{\partial t} + \overline{u_j}\frac{\partial \overline{u_i}}{\partial x_j} = -\frac{1}{\rho}\frac{\partial \overline{p}}{\partial x_i} + \frac{\partial}{\partial x_j}\left[\nu\left(\frac{\partial \overline{u_i}}{\partial x_j} + \frac{\partial \overline{u_j}}{\partial x_i}\right)\right] - \frac{\partial \tau_{i,j}}{\partial x_j} \tag{8}$$

where $\bar{u}_{i,j}$ = velocity component along the flow direction of the resolved scale and p = corresponding pressure. Here, the Reynolds stress is considered as SGS tensor, which is expressed as following-

$$\tau_{i,j} = \overline{u_{i,j}u_{i,j}} - \overline{u_{i,j}u_{i,j}} \tag{9}$$

For the Smagoinsky-Lilly model, the SGS eddy viscosity is modelled as

$$\mu_t = \rho L_s^2 \sqrt{2\overline{S}_{i,j}\overline{S}_{i,j}} \tag{10}$$

where L_s = min (kd, $C_s(\Delta x \Delta y \Delta z)^{1/3}$) = mixing length for subgride scale; d = distance between the nearest walls; κ = von-Karman constant, and C_s = Smagorinsky coefficients.

3 Mesh Convergence Study

Mesh convergence studies are performed to lower the cost of the simulation without affecting the accuracy of the results. In this study meshes are divided into three categories based on the number of elements, viz., coarse (A, D), medium (B, E), and fine (C, F) (Tables 1 and 2). Coefficient of drag (C_d) and coefficient of lift (C_l) are

Table 1 Mesh convergence study for RANS

Mesh	Element number	C_d	C_l
Coarse (A)	57,430	1.07	0.0693
Medium (B)	141,820	1.180	0.0694
Fine (C)	262,700	1.198	0.0711

Table 2 Mesh convergence study for LES

Mesh	Element number	C_d	C_l
Coarse (D)	281,423	1.089	0.701
Medium (E)	564,440	1.210	0.704
Fine (F)	712,310	1.230	0.721

considered for the convergence test, which are calculated as $C_d = 2F_x/\rho u^2 D$ and $C_l = 2F_y/\rho v^2 D$, where u and F_x denote stream wise velocity and force; v and F_y denote spanwise velocity and force.

From Tables 1 and 2 it can be observed that the difference between the coefficient of lift for coarse and medium meshes, for both RANS and LES, are insignificant (0.14% between A and B; 0.42% between D and E). However, the observed difference between the coefficient of drag for coarse and medium are quite high (10.28% between A and B; 11.11% between D and E). Further investigating, the difference between the coefficient of lift as well as the difference between the coefficient of drag for medium and fine meshes, for both RANS and LES, are negligible (the difference of C_l between B and C is 2.44%, the difference of C_l between E and F is 2.7%, the difference of C_d between B and C is 1.52%, and the difference of C_d between E and F is 1.65%, respectively). Hence, mesh B for RANS and E for LES are considered in this study.

4 Validation

To validate the model, the coefficients of drag and lift obtained in this paper are compared with the coefficients of drag and lift presented by previous researchers. For the validation, coefficients of drag and lift in tandem cylinders are calculated based on Reynolds number, $R_e = 25{,}348$.

At gap ratio $(S/D) = 4$ and Reynolds number $R_e = 25{,}348$, the values of $C_{d1} = 1.1$ and $C_{d2} = 0.45$ for circular cylinder in tandeare obtained in this study, respectively. Similarly, At the gap ratio $(S/D) = 4$ and Reynolds number $R_e = 25{,}348$, the values of $C_{l1} = 0.2$ and $C_{l2} = 0.7$ for circular cylinder in tandem are obtained in this study, respectively (Table 3). This result agree well with the results of [13, 14]

5 Results and Discussions

In this section, all of the configurations for different Reynolds numbers and gap ratios are analyzed. For all of the cases, smallest grid size is chosen as 1.2, 1.5 and 0.30 mm along x, y and z directions, respectively. Time-steps $\Delta t = 0.0001$, 0.0002 and 0.00001 s are used in the simulations and the Courant number is maintained lesser than unity. Melville and Chiew [15] concluded that for getting equilibrium

Table 3 Comparative results for tandem cylinders. C_{d1} and C_{d2} are the drag coefficients at the upstream and the downstream of the cylinder, C_{l1} and C_{l2} are the lift coefficients at the upstream and the downstream of the cylinder, respectively

Researches	R_e	S/D	C_{d1}	C_{d2}	C_{l1}	C_{l2}
Alam et al. [13]	20,000	2	1.05	−0.24	0.03	0.55
	20,000	5	1.22	0.29	0.44	0.71
Kitagawa and Ohta [14]	22,000	2	0.88	0.02	0.13	0.58
	22,000	5	1.17	0.50	0.20	1.00
Present study						
Circular cylinder	25,348	2	1.01	0.32	0.17	0.55
	25,348	3	1.08	0.33	0.19	0.58
	25,348	4	1.10	0.45	0.20	0.70

scour depth in a small-scale laboratory experiment, the experiment should be done for several days. However, the main objective of this study is to compare the flow hydrodynamics around twin piers in between RANS and LES; hence, the test duration is not considered very important.

The flow hydrodynamics around single cylinder are different compared to the flow hydrodynamics around two cylinders. The reason is that the flow at the downstream becomes unsteady and produces different vortex shedding zones in the middle of two cylinders and a discontinuity in the flow pattern is observed. This discontinuity depends on Reynolds number and center to center distance between two cylinders [16]. Zdravkovich [17] described the wake interference in tandem cylinder, where the upstream cylinder behaves as a single body and the wake created around the downstream cylinder is strongly influenced by the upstream cylinder.

Here, simulations have been carried out around two circular cylinders placed in tandem for Reynolds number, $R_e = 25{,}348$ and 126,746 with gap ratio, $S/D = 2$, 3 and 4. The velocity at the inlet is considered as 0.5 m/s and 2.5 m/s. A comparison of flow hydrodynamics simulated by Reynolds Average Navier Stoke simulations (RANS) and Large Eddy Simulations (LES) have been made. In RANS k-ε turbulence model and in LES Smagorinsky-Lilly turbulence model is used. Results of velocity distributions simulated in RANS and LES are displayed in Fig. 1 for Reynolds numbers, $R_e = 126{,}746$.

As can be seen from Fig. 1 that at gap ratio, $S/D = 2$ and Reynold number, $R_e = 126{,}746$, vortices do not shed in the gap in RANS but it starts to form at gap ratio $S/D = 2$ in LES. This process of developing vorticity keeps on moving alternately with the increase of gap ratios, $S/D = 3$ to 4. However, the downstream cylinder interference interacts with this increasing vortex and hence modifying the forces experienced by the two cylinders. For smaller spacing ($S/D = 2$), vortices are not observed in the gap between the cylinders, although, the interaction with the surrounding (bottom or top side) of the downstream cylinder is observed. Whereas, at a higher gap ratio ($S/D = 3$, 4), vortices are affected more by the surrounding (bottom, top and front sides) of the cylinders, which leads to form a chaotic flow in the flow field.

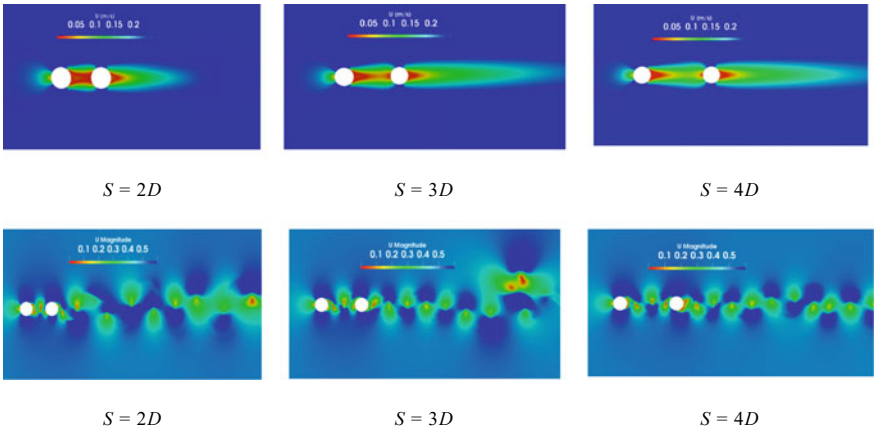

Fig. 1 Velocity variation around tandem cylinders simulated in RANS and LES for circular piers. Upper row is for RANS and lower row is for LES. S = center to center distance of piers, D = diameter of piers. $R_e = 126{,}746$

On the other hand, when fluid particles past by the cylinders, then slow-moving fluid layers create boundary layers. Due to the presence of strong viscosity resistance, flow momentum becomes less in boundary layers. Further increasing the pressure in the flow direction, fluid particles have to overcome this increasing pressure with the addition of high viscosity resistance. Hence, fluid particles either stop or reverse. In this way, fluid layers detached from the solid surface. These separated layers create a high amount of turbulence at the rear side of the cylinder, which is called a wake vortex. It is observed that narrow and wide wakes are generated in the gap region and moved from one cylinder to another cylinder. Streamline plot for Reynolds numbers, $R_e = 25{,}348$ and 126,746 in RANS and LES are shown in Fig. 2, which showed that the flow intensity in the gap region is more complicated than the surroundings of the cylinders. At Reynolds numbers, $R_e = 253$ (laminar flow), a symmetric pattern of streamlines is noticed (not shown here). At Reynolds number, $R_e = 25{,}348$, a series of unsteady pattern is observed in LES. At Reynolds number, $R_e = 126{,}746$, present more comparative results between RANS and LES (Fig. 2). The formation of recirculation zones is noticed earlier in LES than RANS. The random pattern is explained as the irregular breakup of vortices..

The Reynolds number plays a vital role on the wake of two cylinders. Igarashi [18] reported six types of flow pattern in tandem cylinders for $R_e = (0.87\text{–}5.2) \times 10^4$. Similar kind of flow patterns were noticed by [17] at $R_e = 6.0 \times 10^4$.

The only difference in between their observation is that the former found two asymmetric and symmetric vortices in the gap in the cylinders. To study the effect of R_e on the force coefficients in tandem cylinders, simulated in the LES and RANS, a plot of R_e versus C_d and R_e versus C_l is shown in Fig. 3. At low R_e, the variation in the values of C_d and C_l are more in LES than in RANS is observed, whereas at higher R_e the variation in the values of C_d and C_l become negligible. Also, for same

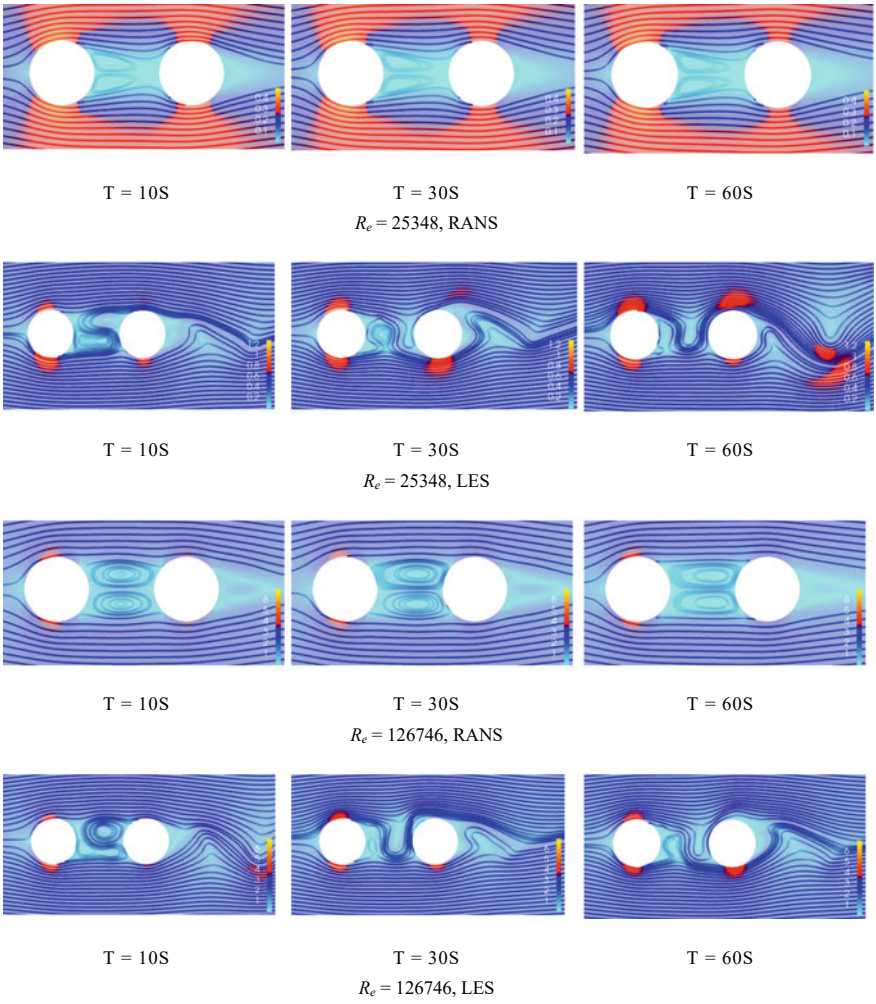

Fig. 2 Evolution of velocity contour for $R_e = 25{,}348$ and $126{,}746$ at the gap $S = 3D$

R_e the values of the coefficients C_d and C_l increase as the gap between the cylinders increases until a critical point ($S = 4D$) is reached, whereafter a fixed value of C_d and C_l are obtained. The force coefficients are calculated in this study as $C_d = 2F_x/\rho u^2 D$ and $C_l = 2F_y/\rho u^2 D$, where F_x is stream-wise force and F_y is spanwise force. The average drag coefficients on the upstream cylinder are about 0.86 in RANS and 0.88 in LES and in the downstream cylinder it is 0.28 in RANS and 0.31 in the LES for $S/D = 2$ and $R_e = 126{,}746$, respectively.

The reason is that the downstream cylinder is affected by the wake of the upstream cylinder, resulting in lower mean drag concerning the upstream cylinder at smaller spacing. Further increasing of spacing, the average drag coefficients on the upstream

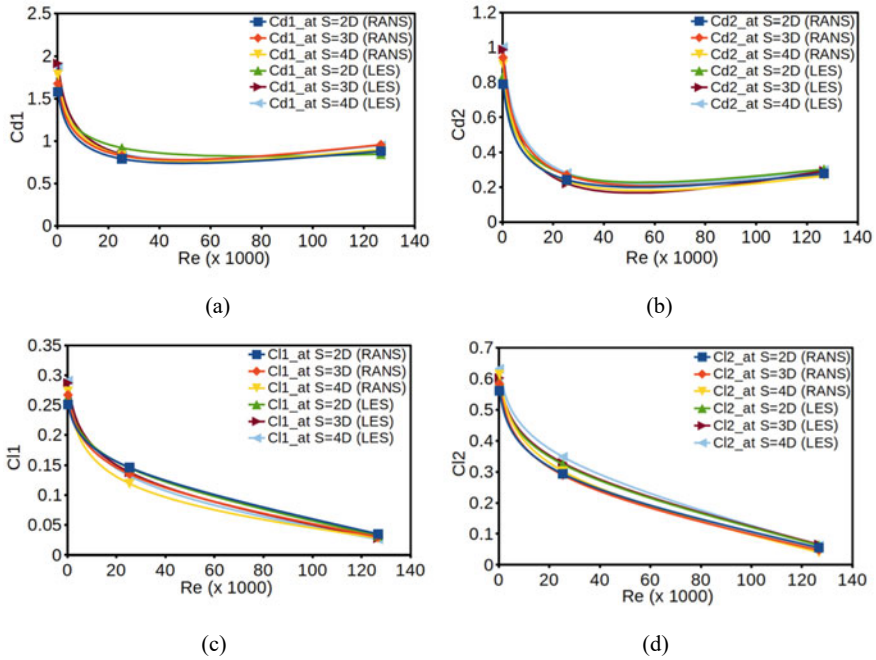

Fig. 3 C_d versus R_e for tandem circular cylinders simulated in RANS and LES

cylinder becomes about 0.89 in RANS and 1.05 in LES and in the downstream cylinder it is 0.29 in RANS and 0.32 in the LES for $S/D = 4$ and $R_e = 126{,}746$, respectively. These results are compatible with the existing experimental data [14].

It is noticed that for smaller spacing ($S/D = 2$), the drag on the first cylinder is almost unaltered in RANS simulation, but in LES alteration in the value is observed. However, the drag on the downstream cylinder is found periodic for both RANS and LES. The present result agreed well with previously existing data. When the spacing in between the cylinder is large ($S/D \geq 4$), vortex shedding from each of the cylinder dominates. This is confirmed by [19]. At smaller spacing, stronger interaction is noticed. The mean value of lift coefficients for a large number of cycles is found to be almost zero at higher spacing. The fluctuation of lift coefficients in RANS is more symmetric than in the LES is also observed. At lower spacing, there is higher pressure in the middle of the cylinders compared to the higher spacing. This makes lower drag on the downstream cylinder at smaller spacing.

Acknowledgements The support from the project of the Institute Scheme for Innovative Research and Development (ISIRD) titled "3D CFD modeling of the hydrodynamics and local scour around offshore structures under combined action of waves and current" from IIT Kharagpur is recognized.

References

1. Derakhshandeh JF, Alam MM (2020) Reynolds number effect on the flow past two tandem cylinders. Wind Struct 30(5):475–483
2. Arif MR, Hasan N (2020) Large-scale heating effects on global parameters for flow past a square cylinder at different cylinder inclinations. Int J Heat Mass Transf 161:120237
3. Arif MR, Hasan N (2019) Vortex shedding suppression in mixed convective flow past a square cylinder subjected to large-scale heating using a non-Boussinesq model. Phys Fluids 31(2):023602
4. Arif MR, Hasan N (2020) Effect of thermal buoyancy on vortex-shedding and aerodynamic characteristics for fluid flow past an inclined square cylinder 38(2):463–471. http://iieta.org/journals/ijht
5. Xu S, Zhou Y, So R (2003) Reynolds number effects on the flow structure behind two side-by-side cylinders. Phys Fluids 15:1214–1219
6. Dey S (2014) Fluvial hydrodynamics. Springer, Berlin
7. Gazi AH, Afzal MS, Dey S (2019) Scour around Piers under Waves: Current Status of Research and Its Future Prospect. Water 11:2212
8. Gazi AH, Afzal MS (2019) A new mathematical model to calculate the equilibrium scour depth around a pier. Acta Geophys 1–7
9. Gazi AH, Purkayastha S, Afzal MS (2020) The equilibrium scour depth around a pier under the action of collinear waves and current. J Marine Sci Eng 8:36
10. Weller HG, Tabor G, Jasak H, Fureby C (1998) A tensorial approach to computational continuum mechanics using object-oriented techniques. Comput phys 12:620–631
11. Jones W, Launder BE (1972) The prediction of laminarization with a two-equation model of turbulence. Int J Heat Mass Trans 15:301–314
12. Rodi W, Mansour N (1993) Low Reynolds number k-ε modelling with the aid of direct simulation data. J Fluid Mech 250:509–529
13. Alam MM, Moriya M, Takai K, Sakamoto H (2003) Fluctuating fluid forces acting on two circular cylinders in a tandem arrangement at a subcritical Reynolds number. J Wind Eng Ind Aero 91:139–154
14. Kitagawa T, Ohta H (2008) Numerical investigation on flow around circular cylinders in tandem arrangement at a subcritical Reynolds number. J Fluids Struc 24:680–699
15. Melville BW, Chiew YM (1999) Time scale for local scour at bridge piers. J Hydraul Eng 125:59–65
16. Mizushima J; Suehiro N (2005) Instability and transition of flow past two tandem circular cylinders. Phys Fluids 17:104107
17. Zdravkovich M (1988) Review of interference-induced oscillations in flow past two parallel circular cylinders in various arrangements. J Wind Eng Ind Aero 28:183–199
18. Igarashi T (1981) *Characteristics of the flow around two circular cylinders arranged in tandem*: 1st report. Bulletin of JSME 24:323–331
19. Prsic MA, Ong MC, Pettersen B, Myrhaug D (2014) Large Eddy Simulations of flow around a smooth circular cylinder in a uniform current in the subcritical flow regime. Ocean Eng 77:61–73